small NANO MICRO

Micromechanics and Advanced Designs for Curved Photodetector Arrays in Hemispherical Electronic-Eye Cameras

Gunchul Shin, Inhwa Jung, Viktor Malyarchuk, Jizhou Song, Shuodao Wang, Heung Cho Ko, Yonggang Huang, Jeong Sook Ha,* and John A. Rogers**

The fabrication of a hemispherical electronic-eye camera with optimized designs based upon micromechanical analysis is reported. The photodetector arrays combine layouts with multidevice tiles and extended, non-coplanar interconnects to improve the fill factor and deformability, respectively. Quantitative comparison to micromechanics analysis reveals the key features of these designs. Color images collected with working cameras demonstrate the utility of these approaches.

Keywords:
- compressible electronics
- elastomeric transfer
- electronic eye cameras
- micromechanics
- silicon membranes

1. Introduction

Digital camera systems that incorporate bioinspired designs can provide certain advantages in imaging compared to conventional devices. One concept involves the use of photodetector arrays on hemispherical surfaces, as analogs to retinas in mammalian eyes, instead of standard planar layouts. From a practical standpoint, such non-planar geometries can be difficult to achieve due to the intrinsically planar nature of established fabrication techniques for electronics/optoelectronics. Approaches to overcome this challenge range from the use of unusual techniques for lithography and related processing on hemispherical surfaces[1,2] to methods for plastically deforming devices formed on flat substrates into spherical shapes.[3] Other strategies involve thin, monolithic silicon structures in planar-mesh geometries that can be subsequently formed into hemispherical shapes.[4,5] A different approach begins with the planar fabrication of organic/inorganic hybrid systems of silicon photodiodes and blocking diodes (i.e., device islands) electrically and structurally interconnected by thin, metal/plastic ribbons, in mesh-type layouts. A hemispherical elastomeric membrane radially stretched into a planar shape receives this mesh upon liftoff from its supporting substrate. Releasing the radial tension causes the elastomer to return to its original, hemispherical shape. This motion places the mesh into a state of mechanical compression at all points across its surface. The interconnection ribbons respond to this compression by lifting out of the plane to form free-standing bridge structures that accommodate the large strain deformations that can be associated with this planar-to-hemispherical geometry transformation. This scheme recently yielded the first electronic-eye cameras capable of collecting images.[6]

Although these ideas provide robust and scalable routes to working systems, important details related to the layouts were not optimized for surface-area coverage of photodetectors (i.e.,

[*] Prof. J. S. Ha, G. Shin
Department of Chemical and Biological Engineering
Korea University
Seoul 136-701 (Korea)
E-mail: jeongsha@korea.ac.kr
Prof. J. A. Rogers, Dr. I. Jung, Dr. V. Malyarchuk, Dr. H. C. Ko[+]
Department of Materials Science and Engineering
Frederick Seitz Materials Research Laboratory and
Beckman Institute for Advanced Science and Technology
University of Illinois at Urbana-Champaign
Urbana, IL 61801 (USA)
E-mail: jrogers@uiuc.edu
Prof. J. Song
Department of Mechanical and Aerospace Engineering
University of Miami
Coral Gables, FL 33146 (USA)
Prof. Y. Huang, S. Wang
Department of Mechanical Engineering
Department of Civil and Environmental Engineering
Northwestern University
Evanston, IL 60208 (USA)
E-mail: y-huang@northwestern.edu

[+] Present address: Department of Materials Science and Engineering
Gwangju Institute of Science and Technology (GIST)
Gwangju 500-712 (Korea)

DOI: 10.1002/smll.200901350

fill factor) or deformability of the array (i.e., to minimize strains in the devices). Here we introduce two new design features, developed in part through the guidance of theoretical mechanics analysis. To improve the fill factor, we use layouts in which each device island supports not just a single photodetector but a cluster of them. We refer to this layout as tiled. To improve the deformability and reduce the strains in the devices we implement extended ribbon interconnects to more effectively accommodate applied forces. Quantitative comparison of key aspects of this mechanics to theory reveals the basic physics. The results, in working camera devices, indicate that these two design modifications double the fill factor, while at the same time reduce the photodetector size by ≈10 times and the strain in the silicon by ≈5–10 times, compared to original designs. Additionally, we implement integrated structures to facilitate connection to external control systems. These ideas and extensions of them could be important for further improvements in cameras of this type, or in other classes of curvilinear electronic/optoelectronic and related systems.

2. Results and Discussion

Figure 1 provides a schematic illustration of the system described here, wrapped onto a hemispherical surface. Each island supports a cluster of four independent silicon photodiodes and current-blocking p–n junction diodes, suitably interconnected for passive matrix readout. The islands connect to nearest neighbors via ribbons consisting of metal layers (Cr/Au) encapsulated by films of polyimide (PI). These ribbons extend from opposing edges of the islands to maximize their lengths for reasons outlined below. In the cameras reported here, the center of the hemisphere supports an 8×8 array of such islands. Metal lines, integrated with the outer regions of mesh structure of the detector array, provide electrical connection to separate image-collection systems. On the periphery of the hemisphere, wiring connects to leads on a printed circuit board (PCB) which, in turn, interface to a control computer via a standard ribbon cable. The enlarged scheme shows a close-packed arrangement of silicon island arrays. Many of the fabrication procedures, including geometry transformation and integration with the hemispherical substrate, are similar to those reported previously.[6] Details appear in the Experimental Section. The tiled layout, compared to one in which each island supports only a single photodetector, clearly improves the fill factor and provides a more scalable route to systems with high pixel counts.

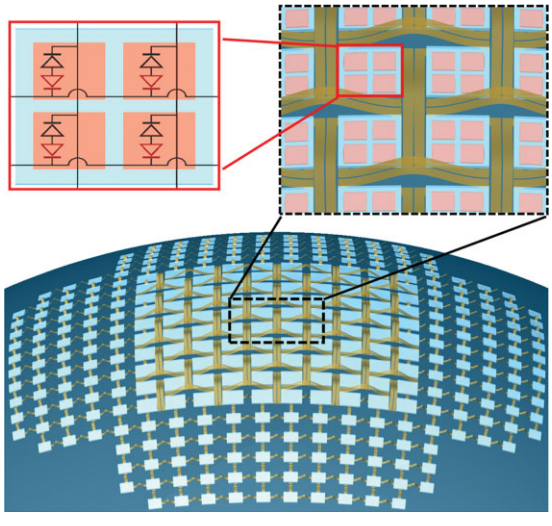

Figure 1. Schematic illustration of an array of interconnected silicon photodetectors in a mesh layout conformally wrapped on a hemispherical substrate (bottom). The top-left frame shows the circuit diagram of an individual island in this mesh, including photodetecting diode (red), a blocking p–n diode (black), and metal interconnection layers (lines). The top-right frame shows that each island supports four silicon photodetector arrays (pink) connected via ribbons (brown) consisting of metal layers (Cr/Au) encapsulated by films of polyimide (PI).

The benefit of the edge-to-edge interconnection scheme can be seen most clearly through mechanics modeling that compares several different designs. Figure 2 shows three schemes, the simplest of which (design 1 in Figure 2a) corresponds to single photodetector islands with center-to-center interconnections, similar to that reported previously.[6] The second design (design 2 in Figure 2b) uses edge-to-edge interconnections, with other features the same as those in Figure 2a. The extended lengths of such interconnections decrease the strain that appears in all parts of the detector array upon transforming the geometry from planar to hemispherical. The third option (design 3), shown in Figure 2c, combines this interconnect strategy with the tiled layout (in this case, four photodetectors per island). This design yields improved fill factor, while retaining enhanced deformability. In all of these figures, gray, yellow, and brown correspond to silicon, polyimide (PI) and metal (Cr/Au), respectively. Each case uses identical dimensions for the silicon ($160 \times 160\ \mu m^2$), the silicon pixel with surrounding polyimide ($220 \times 220\ \mu m^2$), and the pitch (170 μm). Figure 2d provides a cross-sectional view of a part of a single unit cell after transfer to a prestrained (tension) elastomeric substrate of poly(dimethylsiloxane) (PDMS) for which the prestrain has been subsequently relaxed. This process leads to delamination of the interconnect ribbons to form bridge structures, thereby accommodating the compressive strain. The brown layer is Cr/Au encapsulated between PI layers. Such an encapsulated layout places the metals near the neutral mechanical plane for bending.[7] The metal makes contact with the silicon through via holes.

The strains in the interconnect and the island are important design parameters; these quantities can be obtained from mechanics modeling, for different layouts. The interconnects (PI (1.5 μm) /metal (0.16 μm) /PI (1.2 μm), elastic moduli $E_{PI} = 2.5$GPa and $E_{metal} = 78$GPa) are modeled as composite beams with effective tensile rigidity $(Eh)_{bridge}$ and bending rigidity $(EI)_{bridge}$. The neutral plane, shown in Figure 2d, is 0.136 μm from the bottom surface of the metal layer. When the distance between the end points of the interconnect are reduced from the initial value L^0_{bridge} to L_{bridge} upon release of prestrain, the out-of-plane displacement of buckled interconnect takes the form $w = \frac{A}{2}(1 + \cos\frac{2\pi x}{L_{bridge}})$, as illustrated in Figure 3a, where A is an amplitude factor, to be determined by energy minimization. The total energy consists of the bending energy $U_{bending} = (EI)_{bridge}\frac{\pi^4 A^2}{(L^0_{bridge})^3}$ and membrane energy $U_{membrane} = \frac{1}{2}(Eh)_{bridge}[\frac{\pi^2 A^2}{4(L^0_{bridge})^2} - \frac{L^0_{bridge} - L_{bridge}}{L^0_{bridge}}]^2 L^0_{bridge}$.[8]

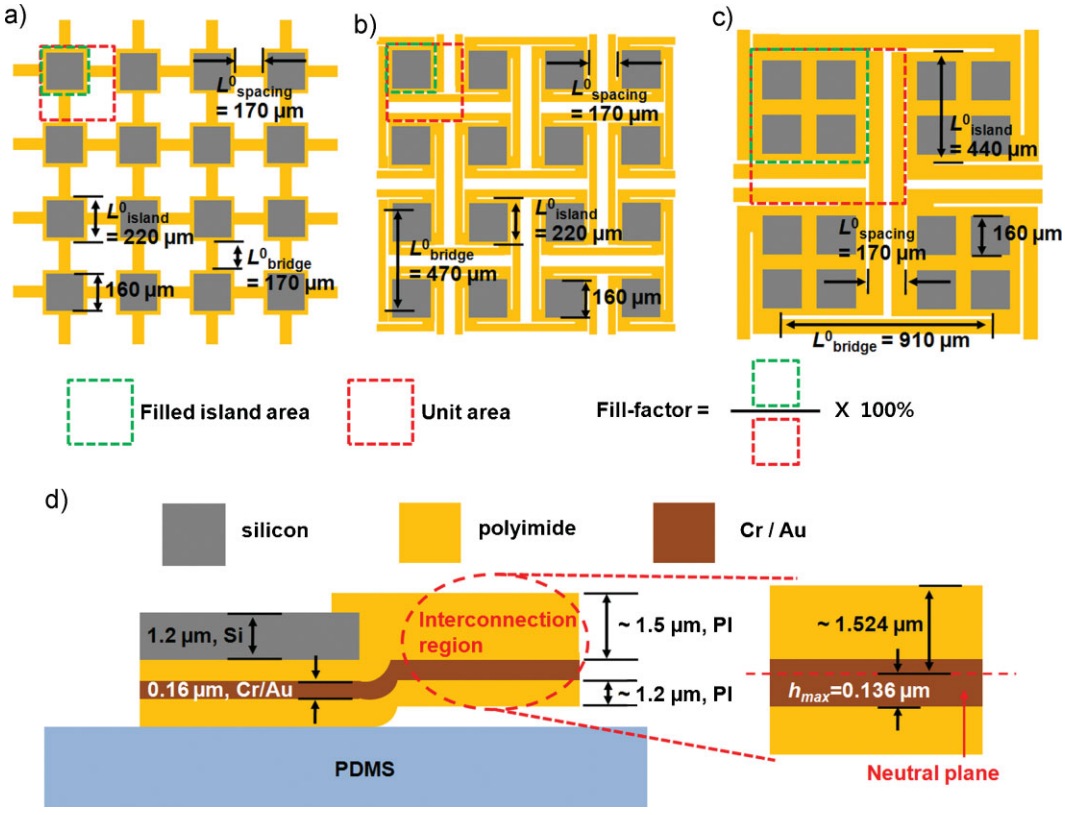

Figure 2. Schematic illustrations of three different design options for photodetector arrays in hemispherical electronic cameras. A single pixel consists of a photodetecting diode and a blocking p–n diode. Interconnection bridges consist of Cr/Au metal layer sandwiched between PI layers. a) Single photodetector island design with center-to-center interconnection bridges. b) Single photodetector island design with edge-to-edge interconnection bridges. c) Multiphotodetector island design (i.e., tiled design) with edge-to-edge interconnection bridges. The dotted green squares and the dotted red squares indicate the filled island area and the unit area used for the calculation of the fill factors, respectively. d) A cross-sectional view of the edge of a representative island, after transfer onto prestrained PDMS and relaxation of this prestrain. The brown layer is Cr/Au, encapsulated by layers of PI.

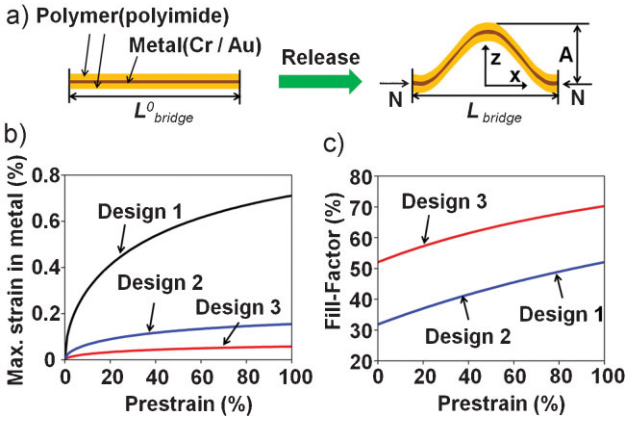

Figure 3. a) Schematic diagram of the mechanics model for interconnection bridges. b) Maximum strain in the metal interconnect layer after release of prestrain for the three different design options illustrated in Figure 2. c) Prestrain-dependent fill factors for these designs.

Energy minimization $\frac{\partial(U_{bending}+U_{membrane})}{\partial A}=0$ gives $A=\frac{2L^0_{bridge}}{\pi}\sqrt{\frac{L^0_{bridge}-L_{bridge}}{L^0_{bridge}}-\varepsilon_c}$, where $\varepsilon_c=\frac{(EI)_{bridge}}{(Eh)_{bridge}}\frac{4\pi^2}{(L^0_{bridge})^2}$ is the critical buckling strain, which is very small when the interconnect length is much larger than its cross sectional dimensions. The length of the island L^0_{island} remains unchanged, while the spacing between islands is reduced from $L^0_{spacing}$ to $L_{spacing}=L^0_{spacing}/(1+\varepsilon_{pre})$, because the prestrain is accommodated almost entirely by buckling of the interconnects. These expressions yield $A\approx\frac{2L^0_{bridge}}{\pi}\sqrt{\frac{\varepsilon_{pre}}{1+\varepsilon_{pre}}\frac{L^0_{spacing}}{L^0_{bridge}}}$, and the strain in the interconnect $\varepsilon=4\pi\frac{h}{L^0_{bridge}}\sqrt{\frac{\varepsilon_{pre}}{1+\varepsilon_{pre}}\frac{L^0_{spacing}}{L^0_{bridge}}}$, where h is the distance from the neutral plane.

For the third design with dimensions shown in Figure 2c subjected to 40% prestrain (spacing reduction of 48.5 μm), the predicted value of A is 133.7 μm, which agrees well with the experimental value of 137.7 μm. The maximum strain in the metal layer occurs at the bottom surface, that is, $h=h_{max}=0.136$ μm. Figure 3b shows the maximum strain in the metal layer of the interconnect versus prestrain for all three designs. The long interconnects in designs 2 and 3 drastically reduce the maximum strain.

The strains in the interconnect and island are proportional to the distance h to the neutral plane, and inversely proportional to the bending stiffness EI.[8] For all three designs shown in Figure 2d, the ratio of h for the position of the silicon to EI of the

interconnect is three times larger than the ratio h for the position of the metal to EI of the island. As a result, the strain in the silicon is one third of the strain in metal and is smaller than that shown in Figure 3b.

The fill factor is the percentage of surface area covered by islands after relaxation. For a unit cell of length $L^0_{\text{island}} + L^0_{\text{spacing}}$, releasing the prestrain changes the length of the unit cell to $L^0_{\text{island}} + L_{\text{spacing}}$. The fill factor is then given as $\beta = (1 + \frac{1}{1+\varepsilon_{\text{pre}}} \frac{L^0_{\text{spacing}}}{L^0_{\text{island}}})^{-2}$, which increases with the prestrain ε_{pre}, and decreases as the ratio $L^0_{\text{spacing}}/L^0_{\text{island}}$ increases. Figure 3c shows the fill factor versus the prestrain for these three designs. Designs 1 and 2 give the same results but design 2 can ultimately reach a larger fill factor because it achieves smaller maximum strain in the interconnects, thereby enabling it to accommodate larger deformation. The fill factor for design 3 is much larger than the other two because it uses a much larger island (i.e., small ratio $L^0_{\text{spacing}}/L^0_{\text{island}}$). As the island size doubles, the fill factor increases from 32% to 52% at zero prestrain, and from 52% to 70% at 100% prestrain. The fill factor varies across the array but at a negligible level for the designs reported here. Detailed theoretical analysis can be found elsewhere.[9]

Figure 4 shows images of a representative tiled extended interconnect system (Figure 2c) on a planar substrate (silicon wafer) immediately after fabrication and after transfer onto the surface of a hemispherical PDMS membrane. The device features and the unit island layout appear in the photograph (Figure 4a) and optical micrograph (Figure 4b), respectively. The interpixel distance in an island is 200 μm while the separation between a pixel in one island and that in a nearest neighbor island is 410 μm. As shown in Figure 4b, the parallel (black arrow) and the perpendicular (red arrow) metal lines connect to blocking diodes and photodiodes, respectively. Figure 4c shows a scanning electron microscopy (SEM) image of the system on a hemispherical PDMS membrane. Every island is well attached to the PDMS while all interconnection ribbons form the expected non-coplanar bridge structures due to release of prestrain (≈40%) in the PDMS. Details of this behavior appear in the zoomed SEM image (Figure 4d). The distribution of prestrain near the top of the hemisphere is approximately equibiaxial.[6] Therefore, the release of prestrain along the ribbon direction causes them to buckle, while the release of prestrain normal to the ribbons moves them closer to one another, in some cases to the point of contact or slightly overlapped (Figure 4d). Although this latter behavior does not affect the functionality of the systems reported here, it can be avoided by slightly increasing the spacing between parallel interconnects. The selective delamination of the ribbons, and not the islands, results from the narrow ribbon width, low bending rigidities, and low adhesion of ribbons to PDMS. We observed no measurable effects of strain on the islands.

Figure 5a shows a completed hemispherical detector array, transferred onto a concave glass substrate mounted on a PCB board with attached ribbon cable for external connection to a computer; a high-resolution optical image of the detector area is also shown. The central square area (4.7 mm×4.7 mm) corresponds to the array of photodetectors; the surrounding regions support electrical wiring pads for external contact to traces on the PCB. Although the solid angle corresponding to

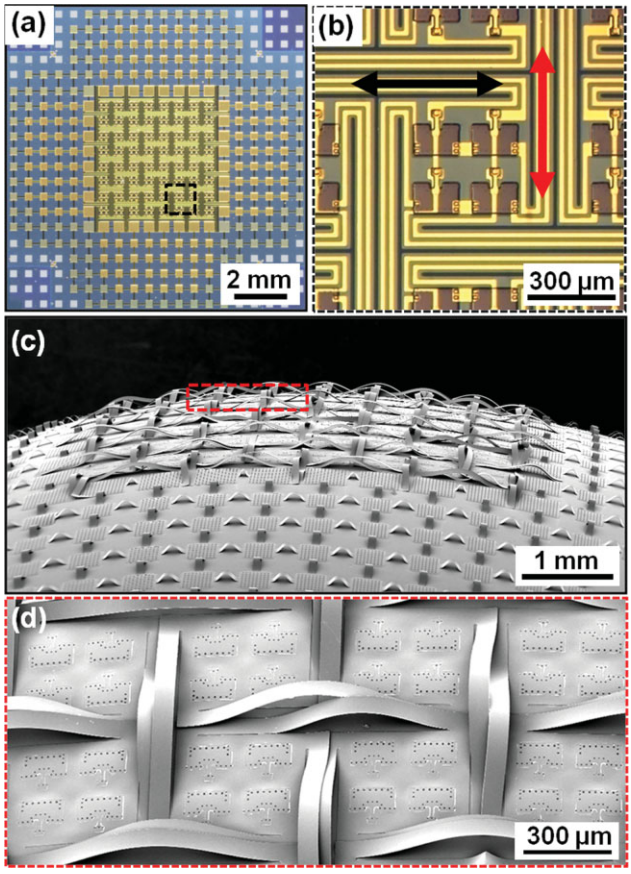

Figure 4. a) Photograph of an integrated detector array using a tiled layout, with edge-to-edge interconnects and integrated wiring to facilitate external electrical connection, in a planar configuration immediately after fabrication. b) Optical micrograph showing a unit cell. The black and red arrows indicate the interconnection bridges to blocking p–n diodes and photodetecting diodes, respectively. c) SEM image of the system on a hemispherical PDMS substrate. d) High-resolution SEM image that highlights the non-coplanar interconnecting bridges.

the photodetector coverage in these hemispherical cameras is modest (≈20°), the same fabrication procedures and mechanics design considerations apply to areas approaching the full hemisphere.

Figure 5b shows the current–voltage (I–V) characteristics of a representative individual photodetector in this hemispherical camera, when the light is on (red line) and off (black line). The data was collected via contacts established at pads terminating at the corresponding row and column electrodes. The back-to-back diode structure (i.e., photodiode/blocking diode) yields a strong photoresponse, with low reverse bias current and low crosstalk between pixels in passive matrix addressing. Blocking diodes are covered with an opaque metal layer to prevent exposure to light, such that a high on/off current ratio (≈100) and a high on/cross talking current ratio (≈300) could be obtained. Image capture involved approaches described previously,[6] with some important modifications. First, due to the layout of interconnects between photodetectors within each island, the order for addressing pixels via the terminating pads does not follow a simple ascending manner. Instead, the real space position of each island was considered

NANO MICRO small

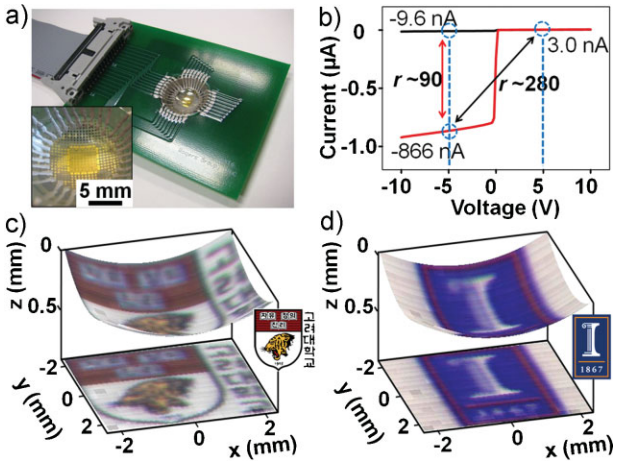

Figure 5. a) Completed hemispherical camera mounted in a PCB board with a connecting ribbon cable. The bottom-left inset provides a view of the hemispherical detector. b) *I–V* characteristics of a representative pixel exposed to light (red) and in the dark (black), respectively. Two important current ratios (*r*) are indicated. Color images of c) Korea University and d) University of Illinois logos obtained using this hemispherical camera. The top, curved surface renderings correspond to the images as collected from the cameras. The bottom, planar versions are projections of the hemispherical images. The illustrations on the right sides of these frames show the patterns that were imaged.

and used to re-order the scanned data. Second, the spacing between pixels in a given island is smaller than that between neighboring islands. To correct this mismatch in distance, scanning was performed based on the spacing of photodetectors in neighboring islands. Some overlapping data were ignored and remaining data were mapped onto the position of each island, based on a photograph of the device (EOS-1Ds Mark III, Canon). The position of each cell in the out of plane direction was calculated based on the lateral position and the radius of hemisphere (12.9 mm). (All of these calibration procedures only need to be performed once.) Third, we exploited sequential data collection through red, green, and blue color filters to construct full-color images. Figure 5c and d shows some results in which the actual images appear in curved surface representations (note the differences between the z and x, y axes) above and planar projections below.

3. Conclusions

This work provides two simple but powerful design modifications in hemispherical detector arrays. Modeling illustrates important mechanical advantages compared to previous work, thereby providing significantly enhanced layouts for imaging. Integrated structures for connection to external control systems facilitate system fabrication. Functioning hemispherical electronic-eye cameras demonstrate the value of these approaches through color pictures of representative patterns and logos. The concepts presented here show the extent to which structural design and mechanics analysis are critically important to hemispherical camera technologies, and more generally to wider ranging classes of deformable, curvilinear devices for applications in biomedicine and other areas. We note that these results do not represent the full extent of optimization that is possible; exploring the limits and also demonstrating the scalability of these approaches to much higher resolution cameras represent valuable directions for future research.

4. Experimental Section

Many of the fabrication details are similar to those described previously.[6] Briefly, the arrays were fabricated via conventional planar processing methods using a silicon-on-insulator wafer (SOI; Soitec, thickness of top Si: 1200 nm, thickness of SiO_2: 400 nm). First, the top -silicon was heavily doped n-type (B219, Filmtronics) and p-type (P506, Filmtronics) using spin-on-dopants in pre-patterned regions. After isolating the silicon pads, the buried oxide of the SOI wafer was removed with HF, leaving the layer raised slightly (≈400 nm) above the underlying silicon wafer, supported by polyimide post structures between the silicon islands. Next, another polyimide layer was spin coated on top and vias were defined for the metal contacts, followed by sputter deposition of Cr(5nm)/Au(150 nm). Finally, another PI layer was coated on top to locate the metal layer near the neutral mechanical plane.[7]

A hemispherical, elastomeric transfer element was molded in PDMS (Sylgard 184, Dow Corning) by casting and thermally curing a bulk quantity of liquid prepolymer to PDMS against a hemispherical glass lens (radius of curvature of 12.9 mm and diameter of 25.4 mm, CVI Laser Optics). Next, the photodetector array mesh was transferred to the PDMS while it was stretched radially into a flat, drumhead shape using a custom-designed mechanical stage. Releasing this applied strain transformed the photodetector array and the transfer element into the original hemispherical shape. Finally, the array was transfer printed onto a matching hemispherical glass lens coated with a thin UV-curable adhesive (NOA 703, Norland). Curing the adhesive and removing the PDMS completed the process.

The system was mounted in a circular opening drilled in a PCB and electrically connected to external pins using silver epoxy. Electrical measurements of individual pixels were performed using a probe station and parameter analyzer (4155c, Agilent). The pictures were collected by illuminating a pattern printed on transparency and paper screen with a backlight. Images were formed on the hemispherical camera by passing the transmitted light through a single plano-convex lens (diameter of 9 mm, focal length of 22.8 mm, JML Optical Industries, Inc). The interface for capturing images was created with National Instruments LabView. The camera was scanned with 10 steps (along two orthogonal rotation axes) between pixels in the detector array using computer-controlled rotation stages.

Acknowledgements

We thank T. Banks for the use of facilities at the Frederick Seitz Materials Research Laboratory. The mechanics and materials of

the work were supported by the National Science Foundation under grant ECCS-0824129 and a MURI award. J.S.H. and G.S. acknowledge Korea Science and Engineering Foundation (KOSEF) through the National Research Laboratory Program funded by the Ministry of Science and Technology (No.ROA-2007-000-20102-0).

[1] H.-C. Jin, M. K. Erhardt, R. G. Nuzzo, J. R. Abelson, *J. Vac. Sci. Technol. B.* **2004**, *22*, 2548.
[2] X. Xu, M. Davanco, X. Qi, S. R. Forrest, *Org. Electron.* **2008**, *9*, 1122.
[3] P. I. Hsu, R. Bhattacharya, H. Gleskova, M. Huang, Z. Xi, Z. Suo, S. Wagner, J. C. Sturm, *Appl. Phys. Lett.* **2002**, *81*, 1723.
[4] P. J. Hung, K. Jeong, G. L. Liu, L. P. Lee, *Appl. Phys. Lett.* **2004**, *85*, 6051.
[5] R. Dinyari, S.-B. Rim, K. Huang, P. B. Catrysse, P. Peumans, *Appl. Phys. Lett.* **2008**, *92*, 091114.
[6] H. C. Ko, M. P. Stoykovich, J. Song, V. Malyarchuk, W. M. Choi, C.-J. Yu, J. B. Geddes III, J. Xiao, S. Wang, Y. Huang, J. A. Rogers, *Nature* **2008**, *454*, 748.
[7] D.-H. Kim, J.-H. Ahn, W.-M. Choi, H.-S. Kim, T.-H. Kim, J. Song, Y. Y. Huang, L. Zhuangjian, L. Chun, J. A. Rogers, *Science* **2008**, *320*, 507.
[8] J. Song, Y. Huang, J. Xiao, S. Wang, K. C. Hwang, H. C. Ko, D. H. Kim, M. P. Stoykovich, J. A. Rogers, *J. Appl. Phys.* **2009**, *105*, 123516.
[9] S. Wang, J. Xiao, I. Jung, J. Song, H. C. Ko, M. P. Stoykovich, Y. Huang, K.-C. Hwang, J. A. Rogers, *Appl. Phys. Lett.* **2009**, *95*, 181912.

Received: July 27, 2009
Revised: December 22, 2009
Published online: March 4, 2010